

# The effect of overlying absorbing aerosol layers on remote sensing retrievals of cloud effective radius and cloud optical depth

By JIM M. HAYWOOD<sup>1\*</sup>, SIMON R. OSBORNE<sup>1</sup> and STEVEN J. ABEL<sup>2</sup>

<sup>1</sup>Met Office, Exeter, UK

<sup>2</sup>Department of Meteorology, University of Reading, UK

(Received 13 June 2003; revised 8 December 2003)

## SUMMARY

Two types of partially absorbing aerosol are included in calculations that are based on intensive aircraft observations: biomass burning aerosol characterized during the Southern AFricAn Regional science Initiative (SAFARI 2000) and mineral dust aerosol characterized during the SaHAran Dust Experiment (SHADE). Measurements during SAFARI 2000 reveal that the biomass burning aerosol layer is advected over the South Atlantic ocean at elevated altitudes above the marine boundary layer which is capped by semi-permanent stratocumulus cloud sheets. Similarly, the mineral dust is measured at elevated altitudes during SHADE resulting in transport above cloud for distances of several thousands of kilometres. We perform theoretical calculations of the effect of these partially absorbing aerosol layers on satellite retrievals of cloud effective radius and cloud optical depth, and show that, in these cases, retrievals of cloud optical depth or liquid water path are likely to be subject to systematic low biases. The theoretical calculations suggest that the cloud effective radius may be subject to a significant low bias for Moderate resolution Imaging Spectrometer (MODIS) retrievals that rely on the 0.86 and 1.63  $\mu\text{m}$  radiance pair for an overlying aerosol layer of either biomass burning aerosol or mineral dust. Conversely, the cloud effective radius may be subject to a significant high bias for Advanced Very High Resolution Radiometer or MODIS retrievals that rely on the 0.63 and 3.7  $\mu\text{m}$  radiance pair for an overlying aerosol layer of mineral dust. Analysis of 1 km resolution MODIS data for the SAFARI 2000 period suggests that the effective radius derived from the 0.86 and 1.63  $\mu\text{m}$  radiance pair is, indeed, subject to a low bias in the presence of overlying biomass burning aerosol. These results show the difficulties associated with remote sensing retrievals, which must be kept in mind when attempting to assess any potential indirect effect.

KEYWORDS: Biomass burning Indirect effects Microphysics Radiation

## 1. INTRODUCTION

Aerosols affect the radiative balance of the earth–atmosphere system via the direct effect whereby they scatter and absorb solar and terrestrial radiation, and via the indirect effect whereby they modify the microphysical properties of clouds thereby affecting their radiative properties and lifetimes. When a partially absorbing aerosol, such as biomass burning aerosol or mineral dust, exists over a dark/bright surface the direct radiative effect is negative/positive; i.e. the local planetary albedo is increased/decreased (e.g. Haywood and Boucher 2000; Keil and Haywood 2003, Hsu *et al.* 2003). Thus, the presence of a partially absorbing aerosol above bright underlying stratocumulus may reduce the spectral irradiances at the top of the atmosphere (TOA).

Retrievals of cloud effective radius,  $r_e$ , and optical depth,  $\delta_{\text{cloud}}$ , from satellite instruments, such as the Advanced Very High Resolution Radiometer (AVHRR) or the Moderate resolution Imaging Spectrometer (MODIS), use the fact that upwelling radiances at wavelengths of less than  $\sim 1 \mu\text{m}$  provide information primarily on  $\delta_{\text{cloud}}$ , intermediate wavelengths around 1–2.5  $\mu\text{m}$  provide information on both  $\delta_{\text{cloud}}$  and  $r_e$ , while those at wavelengths greater than  $\sim 2.5 \mu\text{m}$  provide information primarily on  $r_e$  (e.g. Han *et al.* 1994, 1998; King *et al.* 2003, Platnick *et al.* 2003). These retrievals use look-up tables built up from theoretical radiative transfer models including clouds for different solar zenith angles and viewing-geometry combinations. However, while these theoretical models include gaseous absorption and Rayleigh scattering, they do not include the scattering and absorption by aerosol, because the aerosol optical depth,

\* Corresponding author: Observational Research, Met Office, FitzRoy Road, Exeter, Devon EX1 3PB, UK.

e-mail: jim.haywood@metoffice.com

© Crown copyright, 2004.

$\delta_{\text{aerosol}}$ , the optical parameters and the vertical profile of the aerosol are all essentially unknown. In addition  $\delta_{\text{aerosol}}$  is likely very much smaller than  $\delta_{\text{cloud}}$ , and therefore it might be assumed that including aerosol should not significantly affect the radiances or the retrievals of  $\delta_{\text{cloud}}$  or  $r_e$ .

We investigate two cases here: the case of a biomass burning aerosol layer overlying stratocumulus off the coast of Namibia/Angola during SAFARI 2000, and the case based on measurements made during the SaHARAN Dust Experiment (SHADE) when mineral dust from a Saharan dust outbreak overlies low-level cloud. Both case-studies use *in situ* measurements of the aerosol physical and optical properties. Details of the optical properties of these aerosols are given in section 2, section 3 reports the typical vertical profiles of the aerosol layer and cloud during the measurement campaign, and section 4 provides details of the radiative transfer calculations. Section 5 analyses the theoretical results and section 6 uses MODIS level-2 data products (assigned as MOD06 products; Platnick *et al.* (2003)) to assess whether the theoretical biases are present in the MODIS data. Section 7 presents a discussion and conclusions.

## 2. AEROSOL OPTICAL PROPERTIES

The single scattering albedos,  $\omega_0$ , at a wavelength,  $\lambda$ , of  $0.55 \mu\text{m}$  for biomass burning aerosol and Saharan dust are both derived from *in situ* measurements of scattering measured by a TSI 3563 nephelometer and absorption measured by a Radiance Research Particle Soot Absorption Photometer. The wavelength-dependence of the optical parameters are obtained using log-normal fits to mean aerosol size distributions measured using a Passive Cavity Aerosol Spectrometer Probe (PCASP-100X) combined with suitable refractive indices and Mie scattering theory (Haywood *et al.* 2003a,b). The imaginary part of the refractive index at  $0.55 \mu\text{m}$  is assumed to be  $0.018i$  for biomass burning aerosol and  $0.0015i$  for Saharan dust aerosol (Haywood *et al.* 2003a,b).

For biomass burning aerosol measured during the SAFARI 2000 campaign, three log-normal distributions are used to fit the size distribution representative of aged regional haze as in Haywood *et al.* (2003a). The campaign mean for aged regional haze suggest a  $\omega_{0\lambda=0.55}$  of  $0.91 \pm 0.04$ , a specific extinction coefficient,  $k_{e\lambda=0.55}$ , of  $5.0 \text{ m}^2\text{g}^{-1}$  and an asymmetry factor,  $g_{\lambda=0.55}$ , of  $0.59$ . We show the wavelength-dependence of these parameters in Fig. 1(a), and report the values of the optical parameters at specific AVHRR and MODIS wavelengths in Table 1. When optical parameters determined in this way are included in radiative transfer calculations, the modelled angular distribution of the sky radiance has been shown to be in excellent agreement with independent measurements (Haywood *et al.* 2003c) at wavelengths in the range  $0.55\text{--}2.01 \mu\text{m}$ . This suggests that the optical parameters for biomass burning aerosol are sufficiently accurate in representing the transfer of atmospheric radiation.

For Saharan dust measured during the SHADE campaign, five log-normal distributions are used to fit the size distribution measured during the dust outbreak off the coast of Senegal on 25 September 2000 as in Haywood *et al.* (2003b). While the PCASP enables determination of the aerosol size distribution for particle radii  $<1.5 \mu\text{m}$ , there is a significant contribution to scattering and absorption at solar and near infrared wavelengths from super-micron particles. This necessitates the use of surface-based sun-photometers in determining the super-micron aerosol size distribution (Haywood *et al.* 2003b). Mineral dust may have a significant effect on radiation at terrestrial wavelengths  $>3 \mu\text{m}$  (Highwood *et al.* 2003), although there is considerable uncertainty in the real and imaginary refractive index at these wavelengths (Sokolik *et al.* 1998). Although Highwood *et al.* (2003) showed that the refractive indices of Fouquart *et al.* (1987)

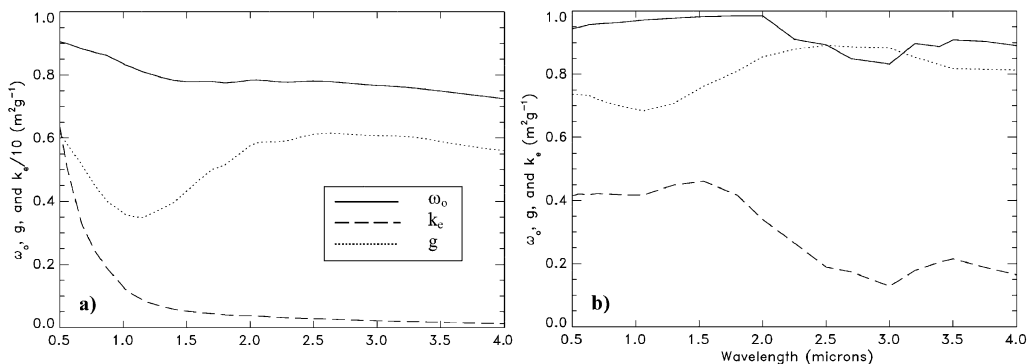


Figure 1. Graph showing the optical properties of: (a) the biomass burning aerosol, and (b) the Saharan dust aerosol used in the calculations. Here  $\omega_0$  is the single scattering albedo;  $g$  is an asymmetry factor and  $k_e$  the specific extinction coefficient. In (a)  $k_e$  has been divided by a factor of ten for ease of graphical representation.

TABLE 1. THE OPTICAL PARAMETERS FOR BIOMASS BURNING AEROSOL (BB), AND SAHARAN DUST AT WAVELENGTHS,  $\lambda$ , USED IN THE RADIATIVE TRANSFER CALCULATIONS

	$\lambda = 0.55$			$\lambda = 0.63$			$\lambda = 0.87$			$\lambda = 1.63$			$\lambda = 2.13$			$\lambda = 3.7$		
	$\omega_0$	$g$	$k_e$	$\omega_0$	$g$	$k_e$												
BB	0.91	0.59	5.00	0.88	0.52	3.90	0.86	0.40	3.50	0.78	0.48	0.50	0.78	0.79	0.40	0.75	0.57	0.20
Dust	0.95	0.74	0.42	0.96	0.73	0.42	0.96	0.70	0.42	0.98	0.78	0.44	0.94	0.86	0.30	0.90	0.82	0.24

The specific extinction coefficient,  $k_e$ , is given in  $\text{m}^2\text{g}^{-1}$ . In the calculations, the aerosol optical depth,  $\delta_{\text{aerosol}}$ , is set to 0.5 at a wavelength of  $0.55 \mu\text{m}$ ; thus  $\delta_{\text{aerosol}\lambda}$  can be approximated as  $0.1k_{e\lambda}$  for biomass burning aerosol, and  $1.2k_{e\lambda}$  for Saharan dust aerosol.

better represent the absorption and scattering of Saharan dust in the 8–12  $\mu\text{m}$  atmospheric window; these refractive indices are only available for wavelengths  $>4.5 \mu\text{m}$ . Therefore the refractive indices of dust from WMO (1986) are assumed for radiative calculations performed at  $3.7 \mu\text{m}$ . The modelled aerosol optical parameters suggest a  $\omega_{0\lambda=0.55}$  of  $0.95 \pm 0.04$ ,  $k_{e\lambda=0.55}$  of  $0.42 \text{ m}^2\text{g}^{-1}$  and  $g_\lambda$  of 0.74 at  $\lambda = 0.55 \mu\text{m}$ . We show the wavelength dependence of these parameters in Fig. 1(b), and report the values of the optical parameters at specific AVHRR and MODIS wavelengths in Table 1. It is interesting to note that  $\omega_0$  increases at wavelengths between 0.55 and  $2.0 \mu\text{m}$ , reaching a value of 0.98 at  $2.0 \mu\text{m}$ . Note here that spherical particles are assumed in determining the radiative properties and radiative effects; the effects of non-sphericity are beyond the scope of the present work.

For Saharan dust  $\omega_{0\lambda=0.55}$  is greater than for biomass burning, indicating that Saharan dust is less absorbing because it does not contain black carbon which is the major absorbing component of atmospheric aerosol (e.g. Haywood and Boucher 2000). One of the most notable differences between Figs. 1(a) and (b) is that  $k_e$  is a strong function of wavelength for biomass burning aerosol (Fig. 1(a)), while for mineral dust it shows much less variation across the range of wavelengths (Fig. 1(b)). This difference is due to the fact that the Saharan dust size distribution contains proportionally more large particles, and this is important when interpreting the results presented in section 5.

### 3. VERTICAL DISTRIBUTION OF AEROSOLS AND CLOUDS

The Met Office C-130 aircraft flew a total of six dedicated flights off the coasts of Namibia and Angola during the SAFARI 2000 measurement campaign (flight numbers

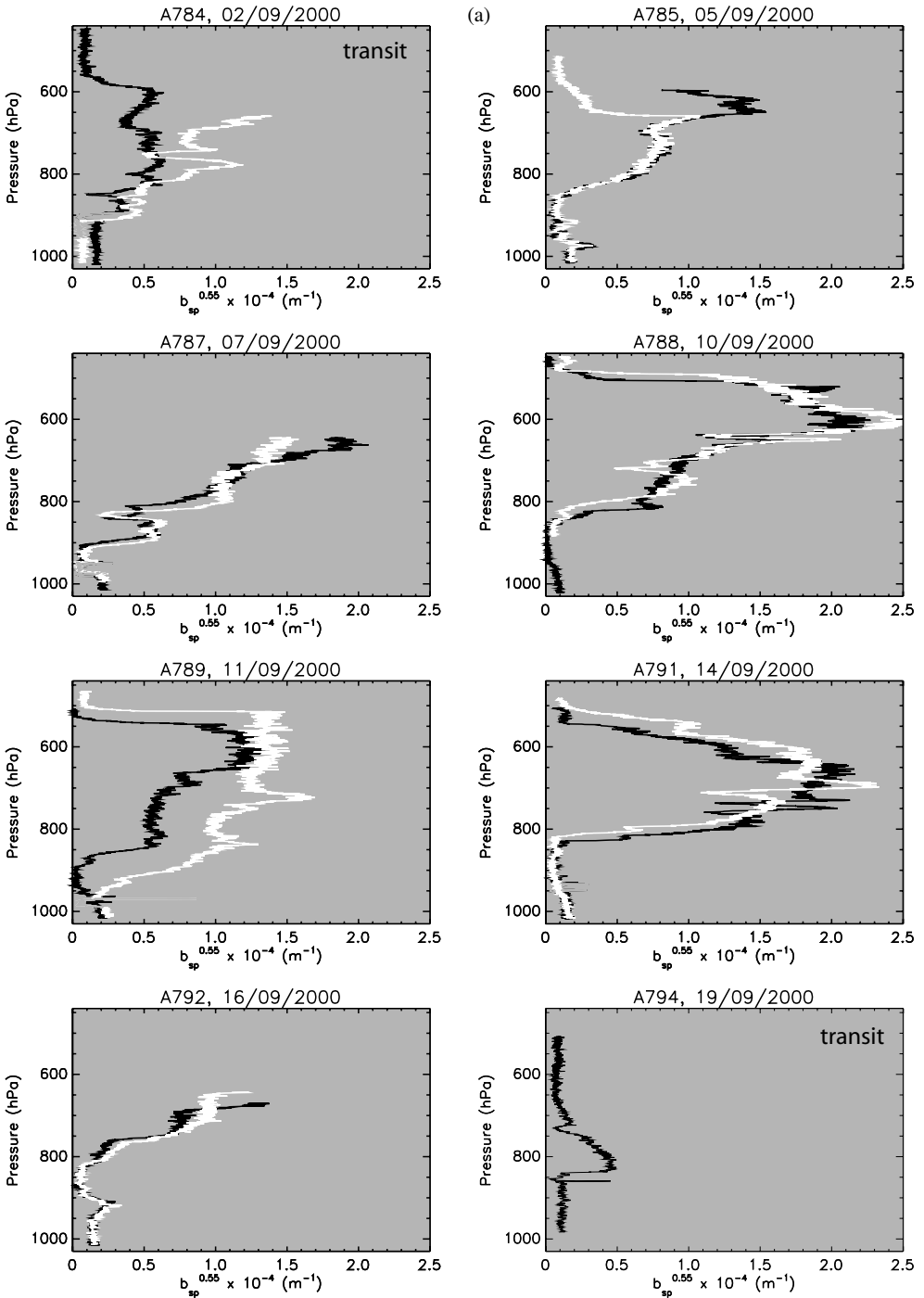


Figure 2. The aerosol scattering coefficient at  $0.55 \mu\text{m}$ ,  $b_{sp}^{0.55}$ , measured by the nephelometer on the C-130 aircraft. Each profile is shown by a separate colour, and in the interests of clarity a maximum of two profiles are shown for each flight. (a) Biomass burning aerosol measured during SAFARI 2000, for eight transit flights as indicated above each frame; (b) Saharan dust aerosol measured during SHADE for six flights. The absolute error in  $b_{sp}^{0.55}$  is estimated as  $\pm 0.3 \times 10^{-4} \text{ m}^{-1}$  for biomass burning aerosol (Haywood and Osborne 2000), but  $\pm 0.5 \times 10^{-4} \text{ m}^{-1}$  for Saharan dust owing to super-micron sampling losses (Haywood *et al.* 2003c). See text for details.

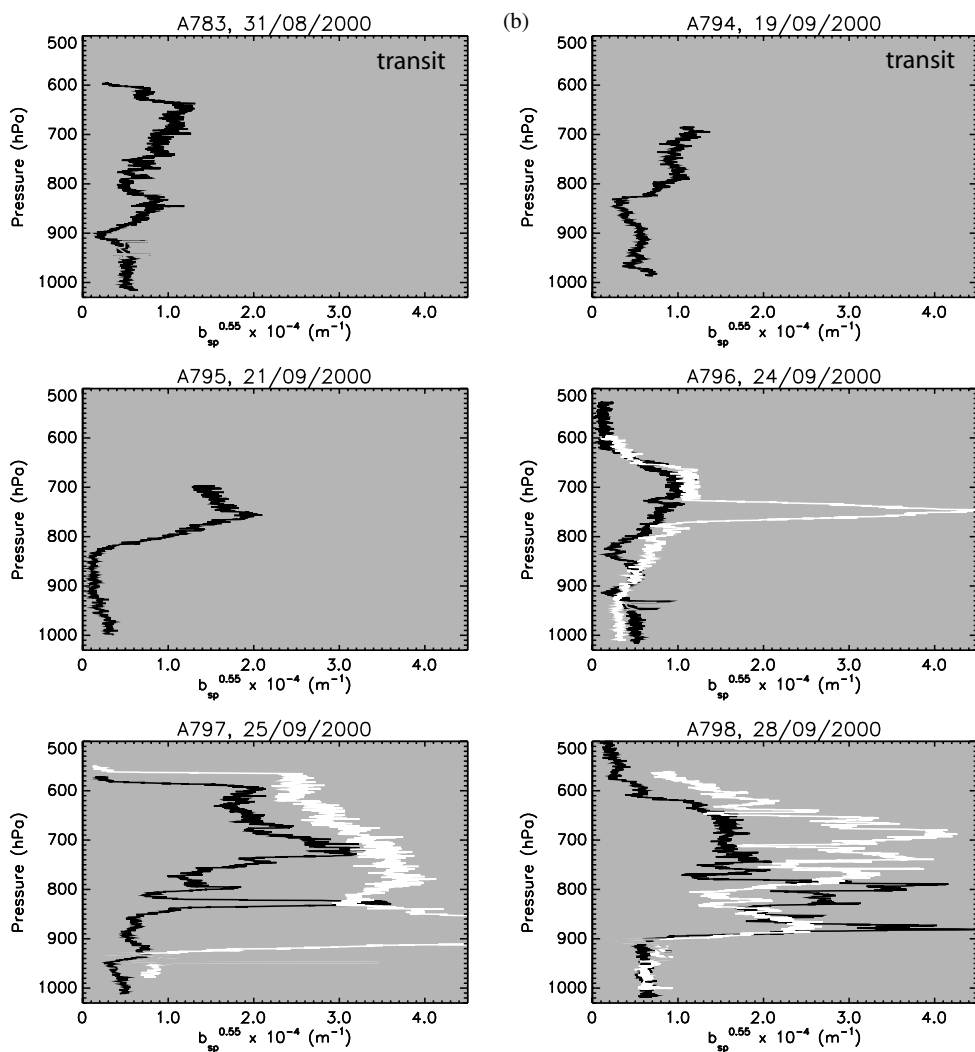


Figure 2. Continued.

a785, a787, a788, a789, a791 and a792). In addition, biomass burning aerosol and stratocumulus cloud were investigated in transit flights to and from Namibia via Ascension Island (a784 and a794). Even at Ascension Island, some 2500 km from the coast of southern Africa, the presence of the biomass burning aerosol layer at elevated altitudes above the marine boundary layer was clear (a794). Figure 2(a) shows a composite of the aerosol volume scattering coefficient at  $0.55 \mu\text{m}$ ,  $b_{\text{sp}}^{0.55}$ , in units of  $\text{m}^{-1}$ , measured by the nephelometer as a function of pressure during profiles flown by the C-130 over ocean. Although the estimated absolute error in  $b_{\text{sp}}^{0.55}$  is  $\pm 0.3 \times 10^{-4} \text{m}^{-1}$ , this error is likely to be systematic and therefore the variability in the profiles is likely to be real. This variability is also revealed in independent measurements on the Convair-580 aircraft and remotely sensed lidar retrievals from the ER-2 aircraft (Kaufman *et al.* 2003). The top of the biomass burning aerosol layer is typically at approximately 500–600 hPa ( $5120 \pm 550 \text{m}$ ), and the bottom of the layer is typically at approximately 800–900 hPa

( $1520 \pm 660$  m). Analysis of the vertical location of stratocumulus clouds reveals that the stratocumulus tops were at around 950 hPa, often separated from the overlying biomass burning plume by a 'clear-slot' (Hobbs 2002; Haywood *et al.* 2003a).

The C-130 performed a total of four dedicated flights from Sal, Cape Verde Islands, during the SHADE campaign (Tanré *et al.* 2003) during the period 21–28 September 2000 (flights a795 to a798). In addition, dust was encountered during profiles on 31 August (a783) and 19 September 2000 (a794) in the vicinity of Sal when the C-130 was travelling to/from Sal–Ascension Island. During the SHADE campaign a large dust storm was advected off the coast of Senegal during the period 24–28 September as shown in Fig. 2(b). The top of the Saharan dust layer was typically 500–600 hPa, which is similar to the situation for biomass burning aerosols shown in Fig. 2(a), while the bottom of the aerosol layer shows considerable variability but is again frequently between 800–900 hPa. Cloud layers were observed at a variety of different levels during SHADE, ranging from small low- to mid-level cumulus to more extensive cloud systems associated with mesoscale systems linked to the intertropical convergence zone (ITCZ). Because of this variability, it is not possible to characterize the typical vertical distribution of clouds in this case.

#### 4. RADIATIVE TRANSFER CALCULATIONS

Radiative transfer calculations were performed using a radiance version of the radiation code of Edwards and Slingo (1996). Typical vertical profiles of humidity, ozone and temperature from the C-130 during SAFARI 2000 were used in the calculations from the surface to approximately 450 hPa; above this level tropical profiles for humidity and temperature from McClatchey *et al.* (1972) were assumed. The exact choice of vertical profiles makes negligible difference to the results. The surface was modelled as a Lambertian surface with constant surface reflectance of 0.05. The use of a more realistic surface parametrization of Glew *et al.* (2004) makes negligible difference to the results. All of the calculations are for nadir views with a solar zenith angle of  $30^\circ$ . Calculations for a solar zenith angle of  $60^\circ$  suggest that the nature of the results in terms of biases is unchanged. Radiative transfer calculations were performed at five wavelengths that are commonly used in retrievals of  $\delta_{\text{cloud}}$  and  $r_e$ , these are: 0.63, 0.86, 1.63, 2.13 and  $3.7 \mu\text{m}$ . The first and last of these wavelengths are used in AVHRR retrievals (e.g. Han *et al.* 1994), while the last four are used in MODIS retrievals (King *et al.* 2003, Platnick *et al.* 2003). For wavelengths of 0.63–2.13  $\mu\text{m}$  the contribution to the TOA upwelling radiances from thermal emission is negligible. For the radiative transfer calculations at  $3.7 \mu\text{m}$ , a realistic sea-surface temperature (SST) of 287 K and a cloud-top temperature of 300 K from aircraft measurements during SAFARI 2000 were assumed; the total TOA upwelling radiance was obtained by summing the solar and terrestrial radiances.

##### (a) Biomass burning aerosol

Having identified that the biomass burning aerosol generally exists above stratocumulus in the region of investigation during the burning season, the effect of biomass burning aerosol overlying stratocumulus on upwelling radiances at TOA was investigated as follows. The stratocumulus cloud droplet distribution was simulated using a log-normal distribution with a fixed geometric standard deviation,  $\sigma$ , of 1.42 ( $\ln \sigma 0.35$ ) which is typical of that found in stratocumulus cloud. The cloud was modelled between 950 and 980 hPa by varying the liquid water content so that  $\delta_{\text{cloud}}$  ranged from 4–20, and by varying  $r_e$  from 4–20  $\mu\text{m}$ . These ranges of  $\delta_{\text{cloud}}$  and  $r_e$  encompass those found off the coast during the measurement campaign in practical terms. Keil and Haywood

(2003) report cloud-top values of  $r_e$  of  $7.4 \pm 3.6$ ,  $7.4 \pm 3.1$  and  $7.8 \pm 1.1 \mu\text{m}$ , and liquid water paths of  $58 \pm 16$ ,  $13 \pm 8$  and  $7 \pm 12 \text{ g m}^{-2}$ , for flights a787, a789, and a793, respectively, suggesting values of  $\delta_{\text{cloud}}$  ranging from 1 to 12. The radiative transfer calculations were repeated including biomass burning aerosol with  $\delta_{\text{aerosol}}$  of 0.5 at  $0.55 \mu\text{m}$  inserted between 900 and 500 hPa (Fig. 2(a)) using the spectrally dependent optical properties shown in Fig. 1(a). Analysis of monthly mean MODIS data (Myhre *et al.* 2003) suggests that a  $\delta_{\text{aerosol}}$  of 0.5 is typical of regions off the coast of Namibia and Angola during September 2000.

### (b) Saharan dust aerosol

Stratocumulus cloud was the dominant cloud type encountered during the SAFARI 2000 mission, and the variability in the vertical profile was relatively modest compared to that encountered during SHADE. It is not possible to characterize typical cloud conditions associated with the presence of Saharan dust events. However, Saharan dust was detected at altitudes above the marine boundary layer, and may be transported over large areas leading to frequent detection in North, Central and South America. In this study, we make the assumption that the underlying cloud consists of stratocumulus with the same characteristics as those modelled in subsection 4(a), and we use the same atmospheric profiles of temperature and humidity and the same SSTs. While these conditions may not be typical, it facilitates a direct comparison of the results from radiative transfer calculations including biomass burning aerosol with those including Saharan dust aerosol. The calculations including Saharan dust aerosol assume a  $\delta_{\text{aerosol}}$  of 0.5 at  $0.55 \mu\text{m}$  inserted between 900 and 500 hPa (Fig. 2(b)) using the spectrally dependent optical properties shown in Fig. 1(b). The  $\delta_{\text{aerosol}}$  value of 0.5 at  $0.55 \mu\text{m}$  is the same as that used for the biomass burning aerosol calculations, which again facilitates comparison. Haywood *et al.* (2003b) show a  $\delta_{\text{aerosol}}$  at  $0.55 \mu\text{m}$  ranging from 0.52 to approximately 1.5 between Sal and Dakar. The highest values of  $\delta_{\text{aerosol}}$  are likely to decrease as the aerosol plume dilutes on moving away from the source regions. It is likely that the size distribution of Saharan dust will evolve during the transport across the Atlantic, with large particles dropping out as a result of sedimentation; this effect is not investigated here.

## 5. RESULTS

We present results both for AVHRR and MODIS retrievals for biomass burning aerosol in subsection (a), and for mineral dust aerosol in subsection (b).

### (a) Biomass burning aerosol

(i) *AVHRR retrievals.* Figure 3(a) shows the TOA  $0.63 \mu\text{m}$  radiance plotted against that for  $3.7 \mu\text{m}$  for the ranges of  $\delta_{\text{cloud}}$  and  $r_e$  discussed in the text. The black lines show the radiances excluding the overlying aerosol; these lines represent those associated with the retrieval algorithms. The white lines show the radiances including the overlying aerosol. The effect of the aerosol upon the  $0.63 \mu\text{m}$  radiance is significant, while there is very little effect upon the  $3.7 \mu\text{m}$  radiance. This can be explained by considering the wavelength-dependence of  $k_e$  (or equivalently  $\delta_{\text{aerosol}}$ ) shown in Fig. 1. While  $\delta_{\text{aerosol}}$  is equal to 0.5 at  $0.55 \mu\text{m}$ , and a still significant 0.39 at  $0.63 \mu\text{m}$ , it is only 0.02 at  $3.7 \mu\text{m}$ . The effect of including aerosol in the calculations is to reduce the  $0.63 \mu\text{m}$  radiance, making the cloud appear less bright. The reduction of the  $0.63 \mu\text{m}$  radiance has important consequences. Consider the point marked A on Fig. 3(a): the retrieval

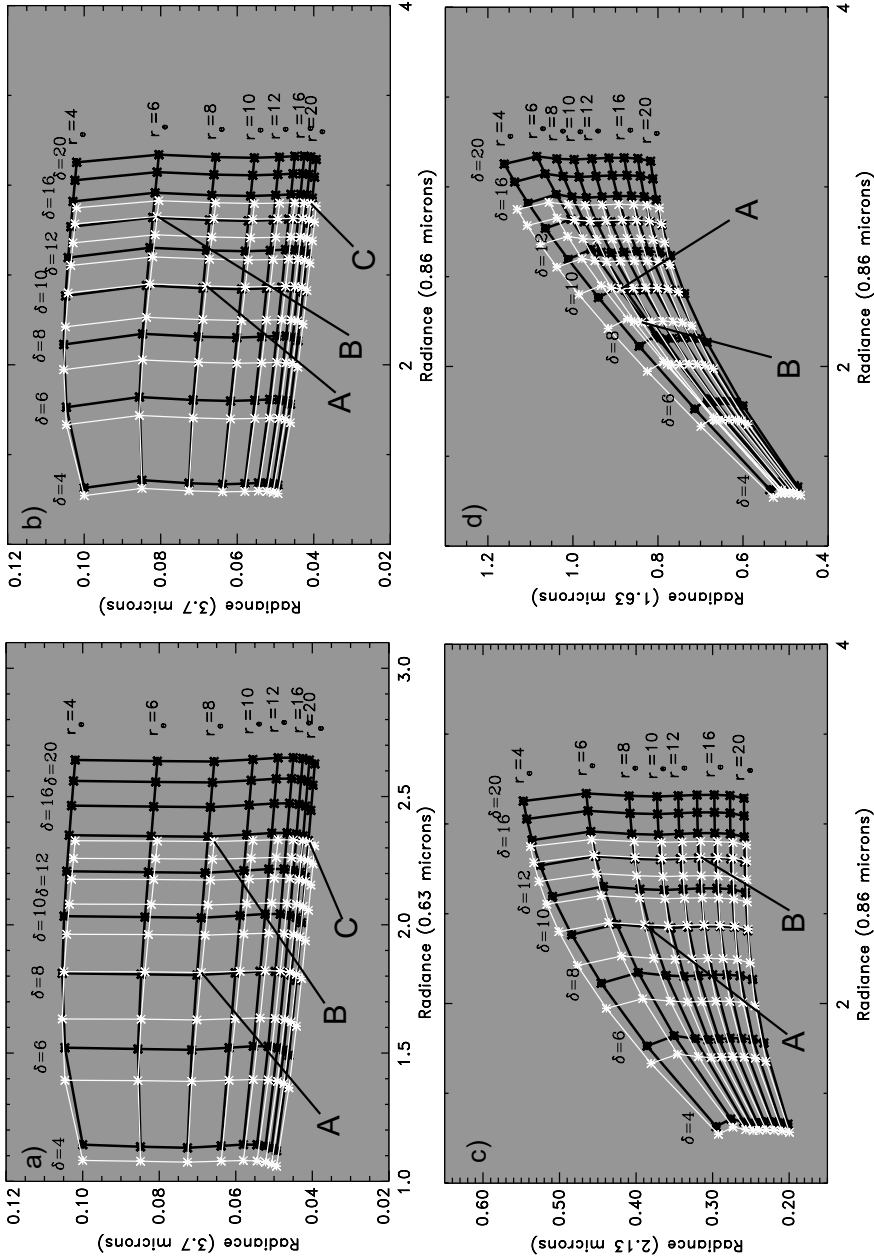


Figure 3. The radiances used in: (a) AVHRR, (b) MODIS retrievals of  $r_{e,c}$ , (c) the default  $r_{e,2.13}$  which is used in obtaining the level-3 MOD08 product, (d) MODIS retrievals of  $\delta_{cloud}$  ( $\delta$  in the figures). The black (white) lines shows results excluding (including) the overlying biomass burning aerosol. The calculations assume a solar zenith angle of  $30^\circ$ , and a Lambertian surface reflectance of 0.05. Letters mark points discussed in section 5. See text for details.

would suggest an apparent  $\delta_{\text{cloud}}$  value of 8, while the actual  $\delta_{\text{cloud}}$  is 10, leading to a 20% bias on the low side. Point B on Fig. 3(a) reveals a low bias larger than 30%, with an apparent  $\delta_{\text{cloud}}$  of  $<14$  while the correct  $\delta_{\text{cloud}}$  is 20. The effect is most pronounced when the aerosol overlies bright clouds with large  $\delta_{\text{cloud}}$ . This effect has been previously documented for TOA irradiances, and radiances for a layer of overlying partially absorbing aerosol (Liao and Seinfeld 1998; Kaufman *et al.* 2001; Hsu *et al.* 2003).

The effects of including overlying partially absorbing aerosols in the retrievals of  $r_e$  are relatively modest, leading to a systematic overestimation of  $r_e$  by less than  $1 \mu\text{m}$  for  $4 < r_e < 12 \mu\text{m}$ . However, when  $r_e$  is  $18 \mu\text{m}$ , an apparent  $r_e$  of  $20 \mu\text{m}$  would be returned by the retrieval as shown by point C on Fig. 3(a).

(ii) *MODIS retrievals.* King *et al.* (2003) and Platnick *et al.* (2003) describe the current operational MODIS retrievals in full, but a brief overview is given here. Over ocean regions, the non-absorbing band of  $0.86 \mu\text{m}$  is used to minimize the effects of Rayleigh scattering. The default retrievals over ocean use the  $0.86 \mu\text{m}$  reflectance in combination with the  $2.13 \mu\text{m}$  reflectance to determine  $\delta_{\text{cloud}}$  and  $r_e$ . In addition, two other retrieval combinations using the  $0.86/1.63$  and the  $0.86/3.7 \mu\text{m}$  reflectance pairs are performed. We adopt the nomenclature of  $r_{e1.63}$ ,  $r_{e2.13}$ , and  $r_{e3.7}$  to represent  $r_e$  determined from the  $0.86/1.63$ ,  $0.86/2.13$  and  $0.86/3.7 \mu\text{m}$  reflectance pairs.

In the level-2 MOD06 cloud product,  $r_{e1.63}-r_{e2.13}$  and  $r_{e3.7}-r_{e2.13}$  are also reported (Platnick *et al.* 2003). The level-3 MOD08 global-gridded (1 degree) cloud product reports daily, 8-day and monthly mean  $\delta_{\text{cloud}}$  and  $r_e$  from aggregations of the default  $2.13 \mu\text{m}$  band retrievals. As the MOD06 products are derived from individual reflectance pairs, we present results from each of the sets of retrievals. We also choose radiances rather than reflectances; reflectances would show identical features.

The results from the  $0.86/3.7 \mu\text{m}$  radiance pair shown in Fig. 3(b) suggest that, as for AVHRR retrievals, there is a significant underestimation of  $\delta_{\text{cloud}}$ . Once again, the effect is greatest for larger  $\delta_{\text{cloud}}$ . Point A highlighted on Fig. 3(b) shows an apparent  $\delta_{\text{cloud}}$  of 10 for a real  $\delta_{\text{cloud}}$  of 12, while the point B shows an apparent  $\delta_{\text{cloud}}$  of 14 for a real  $\delta_{\text{cloud}}$  of 18. The underestimation of  $\delta_{\text{cloud}}$  is therefore not as severe as for AVHRR, because the  $\delta_{\text{aerosol}}$  is 0.39 at  $0.63 \mu\text{m}$  but reduces to 0.20 at  $0.86 \mu\text{m}$  and, therefore, the effect of including the overlying partially absorbing aerosol is not so significant. The effect of including the overlying biomass burning aerosol upon retrievals of  $r_e$  is an underestimate of less than  $2 \mu\text{m}$  (point C) in the parameter space tested here.

The results from the  $0.86/2.13 \mu\text{m}$  radiance pair shown in Fig. 3(c) show similar biases in  $\delta_{\text{cloud}}$  to those shown in Fig. 3(b), with point A showing an apparent  $\delta_{\text{cloud}}$  of 10 for a real  $\delta_{\text{cloud}}$  of 12, while point B shows an apparent  $\delta_{\text{cloud}}$  of 14 for a real  $\delta_{\text{cloud}}$  of 18. The effect of including the overlying aerosol upon retrievals of  $r_e$  is small using these two wavelengths, and does not exceed  $1 \mu\text{m}$  in the parameter space tested here.

The results from the  $0.86/1.63 \mu\text{m}$  radiance pair shown in Fig. 3(d) are perhaps the most interesting. In this case, retrievals of  $\delta_{\text{cloud}}$  are similar to those shown in Figs. 3(b) and (c) when  $0.86$  and  $2.13 \mu\text{m}$  are used, and suggest an apparent  $\delta_{\text{cloud}}$  of 14 for a real  $\delta_{\text{cloud}}$  of 18. However, point A suggests an apparent  $r_e$  of  $\sim 7 \mu\text{m}$  for a real  $r_e$  of  $10 \mu\text{m}$ ; thus the presence of overlying biomass burning aerosol can lead to an underestimate of  $r_e$  that might be interpreted as an ‘apparent indirect effect’, whereby  $r_e$  appears lower than it actually is. The reason that  $r_e$  is affected to a larger degree in the  $0.86/1.63 \mu\text{m}$  radiance pair combination, is that the lines of constant effective radius shown on Fig. 3(d) are less parallel to the  $0.86 \mu\text{m}$  radiance abscissa axis than in the other two cases shown in Figs. 3(b) and (c). Thus a reduction in the  $0.86 \mu\text{m}$  radiance

caused by inclusion of the aerosol moves all the points to the left, while the reduction in the  $1.63 \mu\text{m}$  radiance is fairly small. The white lines of constant real  $r_e$  cross the black lines of constant apparent  $r_e$ . Point B shows an apparent  $r_e$  of  $\sim 5 \mu\text{m}$  for a real  $r_e$  of up to  $10 \mu\text{m}$ , which could lead to serious misinterpretation of  $r_e$ , and consequent differences in the  $r_e$  obtained using the 0.86/1.63 and the default 0.86/2.13  $\mu\text{m}$  radiance pairs.

(b) *Saharan dust aerosol*

(i) *AVHRR retrievals.* Figure 4(a) shows the results from the 0.63/3.7  $\mu\text{m}$  radiance pair. The effect on the 0.63  $\mu\text{m}$  radiance, and hence on the retrieval of  $\delta_{\text{cloud}}$ , is still significant, but not as great as in the case for an overlying biomass burning layer. This is because  $\omega_{0\lambda=0.63}$  and  $g_{\lambda=0.63}$  are higher for Saharan dust than for biomass burning aerosol, resulting in less absorption and more forward scattering by the aerosol. Again, the underestimate is largest for larger  $\delta_{\text{cloud}}$ . The effect of including mineral dust aerosol on the 3.7  $\mu\text{m}$  radiance is much more significant than when biomass burning aerosol is included, because the specific extinction coefficient is still significant at 3.7  $\mu\text{m}$  owing to the presence of large particles (Table 1). The radiance is reduced due to absorption of solar radiation, and also due to absorption and re-emission of terrestrial radiation, where in effect the aerosol is behaving in a similar manner to greenhouse gases (e.g. Highwood *et al.* 2003). This reduction in 3.7  $\mu\text{m}$  radiances has an important consequence: in this case  $r_e$  is overestimated. Point A shows that an apparent  $r_e$  of  $18 \mu\text{m}$  would be retrieved for a real  $r_e$  of  $12 \mu\text{m}$ . Thus the biases in retrievals of  $r_e$  may be either positive (i.e. dust overlying clouds in the AVHRR  $r_{e3.7}$  retrieval) or negative (i.e. biomass burning aerosol overlying clouds in the MODIS  $r_{e1.63}$  retrieval) which further complicates reconciliation of  $r_e$  retrievals using different wavelengths.

(ii) *MODIS retrievals.* Figure 4(b) shows the results from the 0.86/3.7  $\mu\text{m}$  radiance pair; they are similar to those shown in Fig. 4(a) for the AVHRR retrieval. Once again an apparent  $r_e$  of  $18 \mu\text{m}$  would be retrieved for a real  $r_e$  of  $12 \mu\text{m}$  (point A) thus showing that  $r_e$  is overestimated in this case.

Figure 4(c) shows the results from the 0.86/2.13  $\mu\text{m}$  radiance pair. As for biomass burning aerosol, the effect on the 0.86  $\mu\text{m}$  radiance is significant, which leads to the apparent  $\delta_{\text{cloud}}$  being less than the real  $\delta_{\text{cloud}}$ , with a real  $\delta_{\text{cloud}}$  of 20 being interpreted as approximately 16 (e.g. point A). The effect of including Saharan dust above cloud reduces the 0.86  $\mu\text{m}$  radiance less than for biomass burning, despite the fact that  $\delta_{\text{aerosol}\lambda=0.86}$  is 0.50 for Saharan dust and 0.20 for biomass aerosol. This is because  $\omega_{0\lambda=0.86}$  is higher for Saharan dust (less absorption), and because  $g_{\lambda=0.86}$  is higher (less scattering in the backward direction). The underestimate of  $\delta_{\text{cloud}}$  turns into a very small (insignificant) overestimate for a  $\delta_{\text{cloud}}$  value of 4. The mechanism for this changeover from a decrease to an increase in reflectance has been documented for irradiances (e.g. Haywood and Shine 1995, Haywood and Boucher 2000), and is due to the effective surface reflectance decreasing so that the partially absorbing aerosol increases the local planetary albedo. Liao and Seinfeld (1998) document this effect for broadband irradiances for the specific case of mineral dust aerosol above cloud. This mechanism has been suggested to be a plausible method for determining  $\omega_0$  above bright surfaces (Kaufman *et al.* 2001). Figure 4(c) shows that the radiances at 2.13  $\mu\text{m}$  are decreased to a larger extent than the comparable case for biomass burning aerosols (Fig. 3(c)); this is because the wavelength-dependence of  $k_e$  is much less significant for Saharan dust, and thus  $\delta_{\text{aerosol}\lambda=2.13}$  is 0.36 for Saharan dust but only 0.04 for biomass

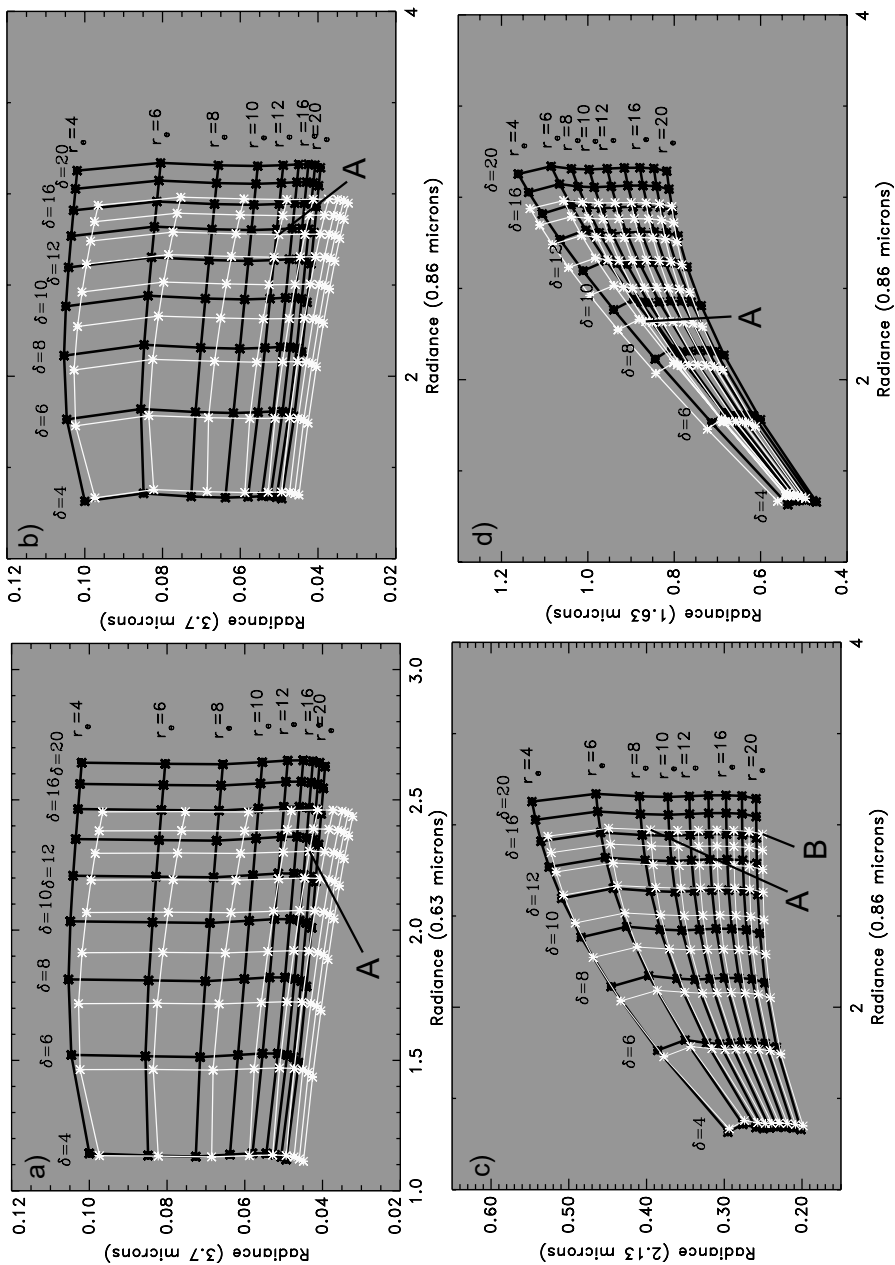


Figure 4. As for Fig. 3 but for Saharan dust aerosol.

burning aerosol. This may lead to a small overestimate of  $r_e$  by up to  $1 \mu\text{m}$  (e.g. point B) for large values of  $r_e$ .

Figure 4(d) shows the results from the  $0.86/1.63 \mu\text{m}$  radiance pair. These results are in many ways similar to those presented for biomass burning aerosol in Fig. 3(d). Once again there is evidence that  $\omega_{0\lambda=1.63}$  is close to the critical value at which the presence of aerosol increases the radiance at low  $\delta_{\text{cloud}}$  but decreases the radiance at high  $\delta_{\text{cloud}}$ . Again an underestimate of  $\delta_{\text{cloud}}$  occurs, and again an underestimation of  $r_e$  occurs whereby an apparent  $r_e$  of  $\sim 5 \mu\text{m}$  is returned for a real  $r_e$  of up to  $10 \mu\text{m}$  (point A), with consequences for remote sensing of the indirect effect.

## 6. EVIDENCE OF THE EFFECT UPON $r_e$ IN MODIS RETRIEVALS

While section 5 has presented the theoretical basis for possible biases in  $\delta_{\text{cloud}}$  and  $r_e$ , no evidence has so far been presented of these biases being present in the actual retrievals. Because  $\delta_{\text{cloud}}$  is essentially determined by just a single radiance ( $0.63 \mu\text{m}$  for AVHRR, and  $0.86 \mu\text{m}$  for MODIS), it is not possible to judge whether there are any differences/biases in  $\delta_{\text{cloud}}$  by analysing the self-consistency of the data; further wavelength-dependent radiance information would be needed and/or analyses of *in situ* aircraft data, which is beyond the scope of this paper. However, as shown in section 5, differences in  $r_e$  derived from the  $0.86/1.63$ ,  $0.86/2.13$  and  $0.86/3.7 \mu\text{m}$  radiance pairs should be evident, and this information is reported in the MOD06 level-2 atmospheric product (subsection 5(a)(ii)). Here we use MODIS data gathered from the Terra platform concurrent with the C-130 aircraft measurements during the SAFARI 2000 period. Stratocumulus clouds were not the prevailing cloud type during the SHADE period, with significant cumulus, cirrus and convective cells associated with the ITCZ all being present in and around the area of investigation. Additionally, while the well-aged biomass burning aerosol showed physical and optical characteristics that did not vary a great deal during the SAFARI 2000 measurement period (Haywood *et al.* 2003a), the aerosol physical and optical properties during SHADE showed significant spatial and temporal variability (Haywood *et al.* 2003b). Therefore, in this investigation we limit ourselves to analysis of the relatively better constrained data from SAFARI 2000.

It is important to realize that in real clouds, where the particle droplet size distribution is a function of geometric height within the cloud, radiances at  $1.63 \mu\text{m}$  are less affected by droplet absorption than those at  $2.13$  and  $3.7 \mu\text{m}$ , and consequently  $r_{e1.63} < r_{e2.13} < r_{e3.7}$ . This is because, in effect, the shorter wavelength radiances are made up of photons scattered from further down in the cloud where the droplet size is typically smaller (e.g. Garrett and Hobbs 1995; Platnick 2000). Keil and Haywood (2003) show the liquid water content and  $r_e$  determined from *in situ* instrumentation during two C-130 profiles on flight a787 on 7 September 2000, and show that the stratocumulus clouds are close to adiabatic in nature with  $r_e$  values of  $\sim 5\text{--}6 \mu\text{m}$  at cloud base and  $\sim 9 \mu\text{m}$  at cloud top. Platnick (2000) performs theoretical calculations investigating differences in  $r_{e1.63}$ ,  $r_{e2.13}$ , and  $r_{e3.7}$  for a range of different vertical profiles of cloud particle size distribution. In all cases for  $5 < \delta_{\text{cloud}} < 15$ ,  $|r_{e1.63} - r_{e2.13}| < |r_{e3.7} - r_{e2.13}|$ ; i.e. the positive difference between  $r_{e3.7}$  and  $r_{e2.13}$  is greater in magnitude than the negative difference between  $r_{e1.63}$  and  $r_{e2.13}$ . In these theoretical calculations,  $|r_{e1.63} - r_{e2.13}|$  and  $|r_{e3.7} - r_{e2.13}|$  are less than  $1 \mu\text{m}$  for the modelled adiabatic cloud, and less than  $1.5 \mu\text{m}$  when the cloud is modelled as sub-adiabatic at mid levels. When MOD06 level-2 data off the coast of South America are analysed by Platnick *et al.* (2003)  $|r_{e3.7} - r_{e2.13}|$  is generally less than  $1 \mu\text{m}$ . However, significant regions exist where  $|r_{e1.63} - r_{e2.13}| > 1$ ,

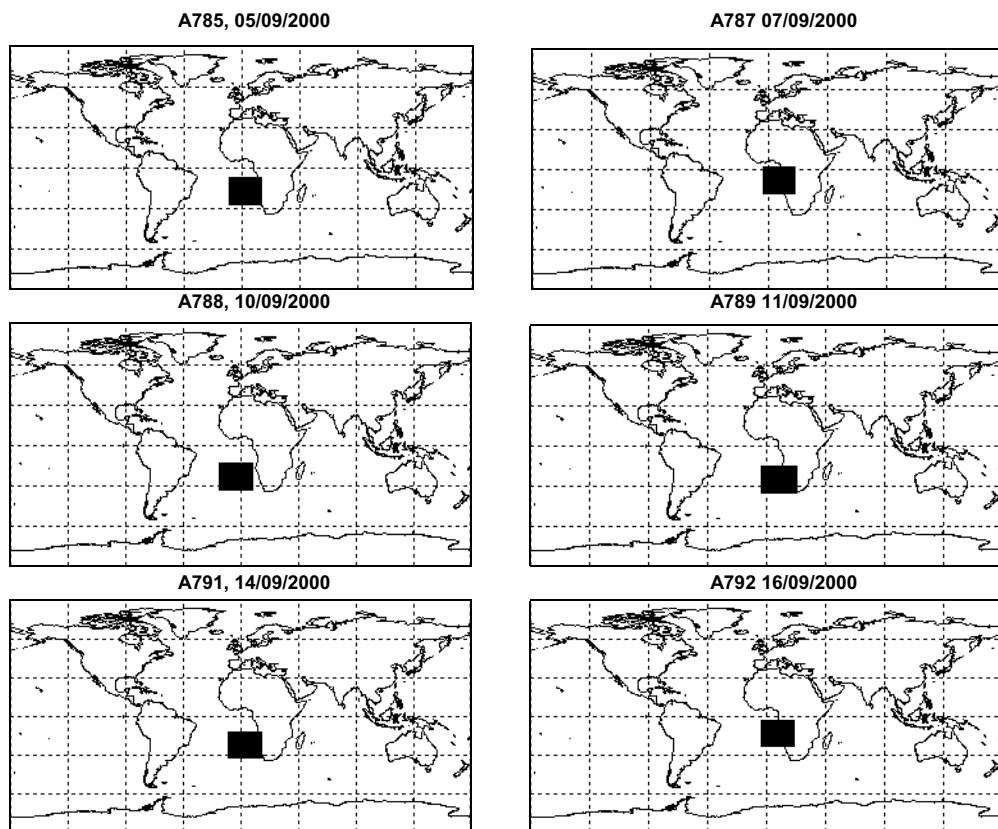


Figure 5. The locations of the granules (see text) of MODIS data shown in the quick-look data in Fig. 6 and satellite retrievals in Fig. 7 for flights as indicated.

and sometimes  $|r_{e1.63} - r_{e2.13}| > 2.5$ , despite the fact that this region should not be influenced by overlying absorbing aerosol. Thus any influence of absorbing aerosol above cloud in the Namibian/Angolan coastal regions on  $r_{e1.63}$  is likely to be in addition to that due to vertical photon transport, which will complicate detection of the theoretical aerosol effect.

The granules\* that are analysed here are available from <http://daac.gsfc.nasa.gov/MODIS/>, and are collocated temporally and geographically with the dedicated aircraft flights (see Fig. 1 in Haywood *et al.* 2003a). The geographic locations of the areas examined here are shown in Fig. 5, and quick-look, real-colour imagery of the scenes that are investigated in detail (September 7 and September 10) are shown in Fig. 6. A cursory examination of Fig. 6 shows the presence of biomass burning smoke aerosol over land regions. An approximate north–south gradient can clearly be seen in Total Ozone Mapping Spectrometer (TOMS) Aerosol Index (AI) data during this period (e.g. Haywood *et al.* 2003a). Smoke is more difficult to distinguish over the ocean regions because of the presence of clouds and areas of sun-glint in some of the data. The areas where smoke aerosol or sun-glint are obviously visually apparent are marked on Fig. 6. Visually, it is difficult to distinguish which cloudy areas are affected by smoke from

\* ‘Granules’ is the technical National Aeronautics and Space Administration term for the data that are analysed, not the results of the analysis.

the MODIS quick-look images, and a more detailed quantitative knowledge of the areas affected by high concentrations of aerosols is required. Here we use the TOMS AI data (<http://toms.gsfc.nasa.gov/aerosols/aerosols.html>) from the same day as that on which the MODIS data were collected. The TOMS and the MODIS instruments are on different satellite platforms, and therefore the aerosol will not be in exactly the same locations due to advection. However, we make the reasonable assumption that the advection rate is relatively small. It would theoretically be possible to determine the regions affected by aerosol by analysing the MODIS MOD04 aerosol products, but  $\delta_{\text{aerosol}}$  may only be determined in cloud-free conditions and thus calculations of  $\delta_{\text{aerosol}}$  and  $\delta_{\text{cloud}}$  are mutually exclusive. We prefer to use the TOMS AI data in this analysis because the statistics for  $\delta_{\text{aerosol}}$  from MODIS are comparatively extremely sparse. The TOMS AI does not translate to  $\delta_{\text{aerosol}}$  via a universal linear relationship, but is dependent on the aerosol absorption properties and the altitude of the aerosol. Hsu *et al.* (1999) compared sun-photometer data to aerosol optical depth both for African biomass burning sites and for Saharan dust (Dakar and Cape Verde) sites, and reported an aerosol-type-dependent linear relationship for both cases. For biomass burning the relationship  $\delta_{\text{aerosol}\lambda=0.38} \sim 0.80(\text{TOMS AI})$  was found, while for Saharan dust the relationship  $\delta_{\text{aerosol}\lambda=0.38} \sim 0.35(\text{TOMS AI})$  was found. We convert  $\delta_{\text{aerosol}\lambda=0.38}$  to  $\delta_{\text{aerosol}\lambda=0.55}$  by using the modelled wavelength-dependence of  $k_e$ . The approximate relationships  $\delta_{\text{aerosol}\lambda=0.55} = 0.40(\text{TOMS AI})$  for biomass burning aerosol and  $\delta_{\text{aerosol}\lambda=0.55} \sim 0.36(\text{TOMS AI})$  for Saharan dust are deduced.

The quick-look images of Fig. 6 are shown in detail for 7 and 10 September. These represent two cases where the  $\delta_{\text{aerosol}}$  and the TOMS AI were high, and the area showed significant quantities of cloud in the range  $5 < \delta_{\text{cloud}} < 25$ , values that are consistent with the theoretical analyses. There is a significant difference between the two cases. For 7 September we shall see that the TOMS AIs indicate that there is significant aerosol loading throughout the region (subsection 6(a)); for 10 September there is a significant gradient in TOMS AI indicating the presence of aerosol to the north of the region, but clean, aerosol-free areas to the south (subsection 6(b)). The other four cases are less ideal for a variety of reasons including: lack of stratocumulus cloud, the effects of other types of cloud in the region, lack of aerosol, and/or the effects of sun-glint in the MODIS retrievals; consequently we chose not to present a detailed analysis here. However, we do present statistics that summarize the results from these cases (subsection 6(c)).

#### (a) 7 September 2000

Figure 7(a) shows the TOMS AI over the region. Highest TOMS AIs are evident close to the coast of Angola where the AI exceeds 3.5 ( $\delta_{\text{aerosol}\lambda=0.55}$  exceeds  $\sim 1.4$ ). It is evident that the majority of the region under investigation is influenced by aerosol. Figure 7(b) shows the default  $r_{e2.13}$  for 7 September. The majority of the regions of stratocumulus show  $12 > r_{e2.13} > 5 \mu\text{m}$ . *In situ* measurements of the near-cloud-top  $r_e$ , by instruments on the C-130 between 15 and 17°S off the coast of Angola, reveal  $r_e = 7.4 \pm 3.6 \mu\text{m}$  (Keil and Haywood 2003) and are thus in general agreement with the MODIS data in that area. Figure 7(b) shows the area affected by sun-glint; in this region  $r_e$  is only derived for clouds that are optically thick enough to make the effects of sun-glint negligible. Figure 7(c) shows the difference in effective radius between  $r_{e3.7}$  and the default  $r_{e2.13}$ ,  $r_{e3.7} - r_{e2.13}$ , obtained for 7 September. The theoretical calculations presented in subsection 5(a)(ii) suggest that there should be little influence of overlying aerosol at these wavelengths, and therefore one would expect  $r_{e3.7} - r_{e2.13}$  to be close to zero or slightly positive from parcel theory (Platnick 2000; Platnick *et al.* 2003). This is indeed the case (see Fig. 7(c)), with the majority of areas showing differences of less

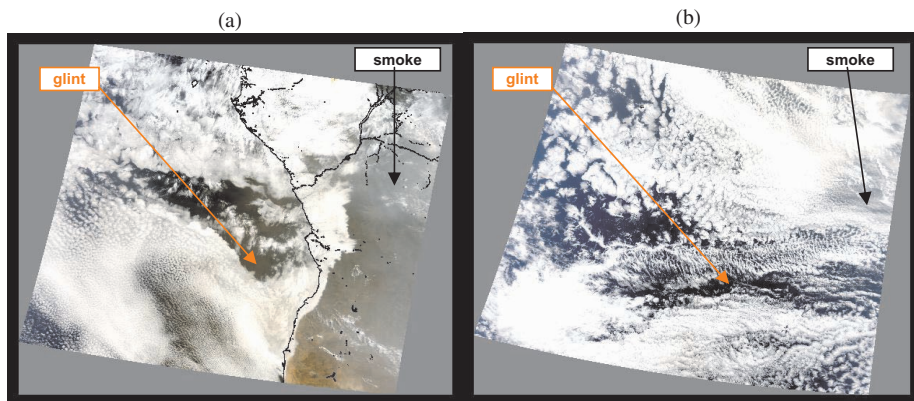


Figure 6. Quick-look data from the MODIS website (<http://daac.gsfc.nasa.gov/MODIS/>) of the areas shown in Fig. 5 for (a) 7 and (b) 10 September 2000. Discernible cloud-free areas with significant aerosol loading and areas of sun-glint are marked as ‘smoke’ and ‘glint’.

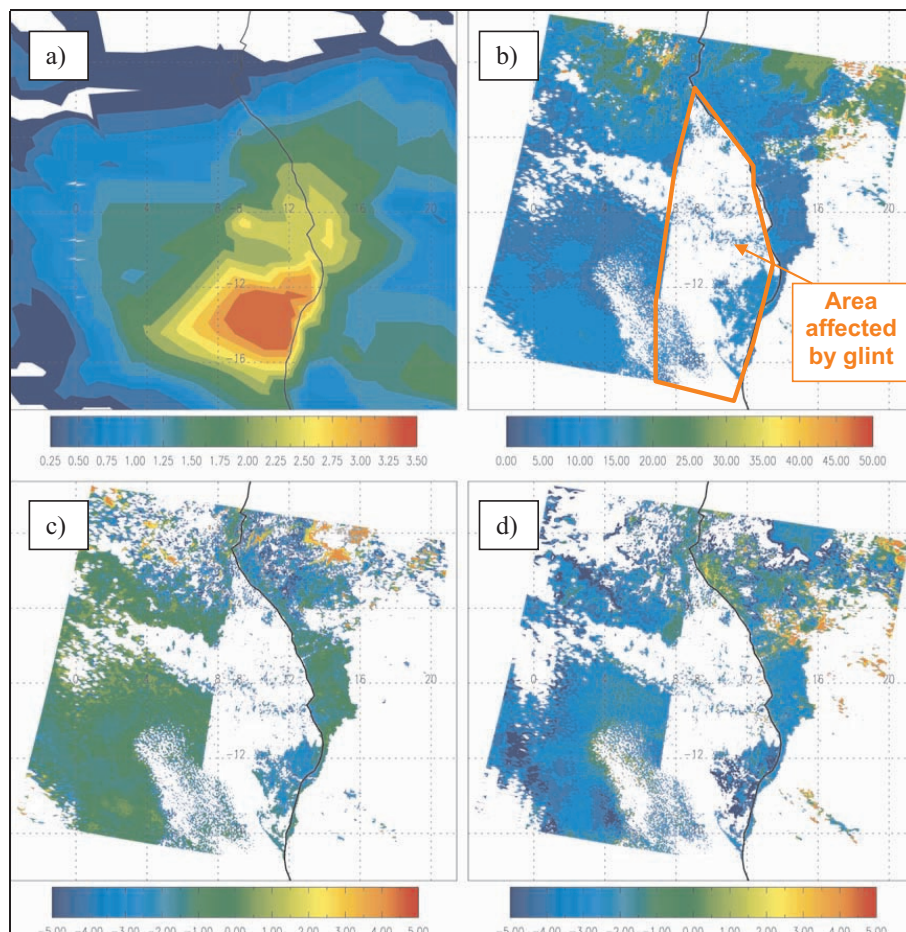


Figure 7. Satellite retrievals for 7 September 2000, over the regions shown in Figs. 5 and 6. (a) TOMS data showing the Aerosol Index (<http://toms.gsfc.nasa.gov/aerosols/aerosols.html>); the data are interpolated in regions outside the TOMS swath; the approximate relationship  $\delta_{\text{aerosol}\lambda=0.55} \sim 0.40\text{TOMS AI}$  applies. (b) The MODIS MOD06 level-2 default  $r_{e2,13}$ , showing the area affected by sun-glint. (c)  $r_{e3.7}-r_{e2,13}$  and (d)  $r_{e1.63}-r_{e2,13}$ . See text for details.

than  $\sim 1 \mu\text{m}$  in magnitude. Some of the northern regions in Fig. 7(c) show yellow and red colours, i.e.  $r_{e3.7} - r_{e2.13} > 2 \mu\text{m}$ ; these are likely to be associated with deep convection and, while important, are not relevant in this study. The blue colours shown in Fig. 7(d) indicate a significant negative difference in  $r_{e1.63} - r_{e2.13}$ . Mid-blue colours represent  $r_{e1.63} - r_{e2.13}$  values of approximately  $-2$  to  $-4 \mu\text{m}$ , and the dark blues represent values ranging from  $-4$  to  $-7 \mu\text{m}$  (the scale ranges to a maximum of  $-5 \mu\text{m}$ ). The theoretical analysis of Platnick (2000) suggests that  $|r_{e3.7} - r_{e2.13}| > |r_{e3.7} - r_{e1.63}|$ , but this is not the case here, which might be an indication that overlying absorbing aerosols are influencing the retrievals. However, the analysis by Platnick *et al.* (2003) of MODIS data off the coast of S. America suggests that  $|r_{e3.7} - r_{e2.13}| < |r_{e3.7} - r_{e1.63}|$ , so we cannot infer that overlying biomass burning aerosol is influencing the retrievals from this feature alone. Indeed, the lack of a spatial gradient in aerosol loading in this case makes it difficult to reach a definite conclusion that overlying biomass burning aerosol is affecting the retrievals. Such a case is provided by 10 September. A more detailed statistical analysis of  $r_{e3.7} - r_{e2.13}$  and  $r_{e3.7} - r_{e1.63}$  in the form of probability density functions (pdfs) is given in subsection 6(c).

### (b) 10 September 2000

Figure 8(a) shows the TOMS AI over the region. In this case a strong spatial contrast is evident, with aerosol affecting the north and particularly the north-east of the region with maximum AIs exceeding 2 ( $\delta_{\text{aerosol}\lambda=0.55} > \sim 0.8$ ). To the south of the region the AI is close to zero. Figure 8(b) shows the default  $r_{e2.13}$  for 10 September; once again the area affected by sun-glint is evident. Typically,  $12 < r_{e2.13} < 5 \mu\text{m}$ , which is similar to the  $r_{e2.13}$  retrievals on 7 September. There is evidence of ice cloud present in the lower left-hand side of the image, shown by  $r_{e2.13}$  reaching  $15\text{--}30 \mu\text{m}$ . Figure 8(c) once again shows that the  $r_{e3.7}$  retrieval is not greatly affected by overlying aerosol, with the majority of regions showing green colours indicating that  $|r_{e3.7} - r_{e2.13}|$  is less than  $1\text{--}2 \mu\text{m}$ . Figure 8(d) shows  $r_{e1.63} - r_{e2.13}$ . To the south of the region there is little difference between the  $r_{e1.63}$  and  $r_{e2.13}$ , and therefore the majority of the south shows green colours associated with  $|r_{e1.63} - r_{e2.13}|$  of less than  $1\text{--}2 \mu\text{m}$ . To the north of the region differences between  $r_{e1.63}$  and  $r_{e2.13}$  become greater in magnitude and hence blue colours become evident. It is clear that the geographic north–south split in  $r_{e1.63} - r_{e2.13}$  appears well correlated with the TOMS AI shown in Fig. 8(a). This piece of evidence supports the theoretical calculations that are presented in section 5, which suggest that  $r_{e1.63}$  is biased to smaller values by the presence of overlying absorbing biomass burning aerosol. Again, a statistical analysis of  $r_{e3.7} - r_{e2.13}$  and  $r_{e3.7} - r_{e1.63}$  is given in subsection 6(c).

### (c) Statistical analysis of the results

An analysis of the MODIS data for 7 and 10 September is given in the form of pdfs in Fig. 9 and Table 2. In determining the data in the pdfs three criteria are applied.

(i)  $5 < \delta_{\text{cloud}} < 25$ . This removes clouds with large optical thicknesses such as convective cloud, and the results should be consistent with the theoretical calculations performed in sections 4 and 5.

(ii) *Cloud over land areas is screened out.* This is because over land areas the aerosol tends to be well-mixed throughout the boundary layer (Haywood *et al.* 2003a), and the relative vertical position of aerosol and cloud cannot be assured.

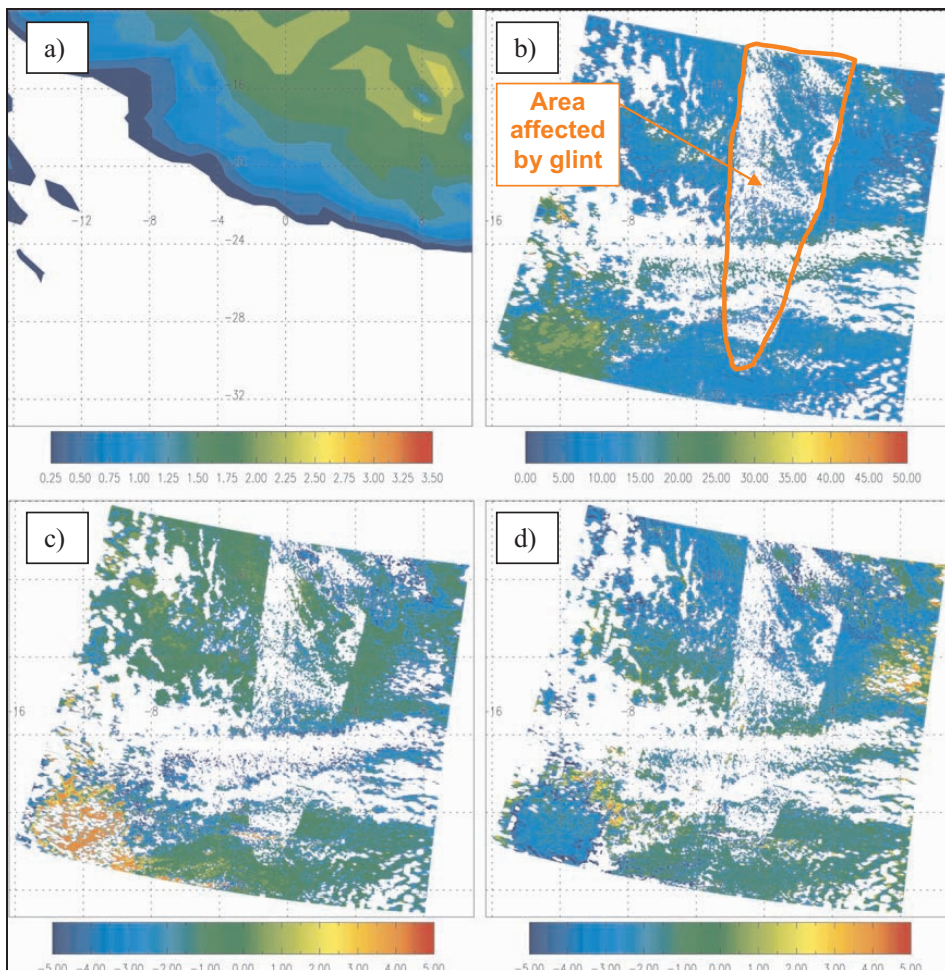


Figure 8. As for Fig. 7 but for 10 September 2000.

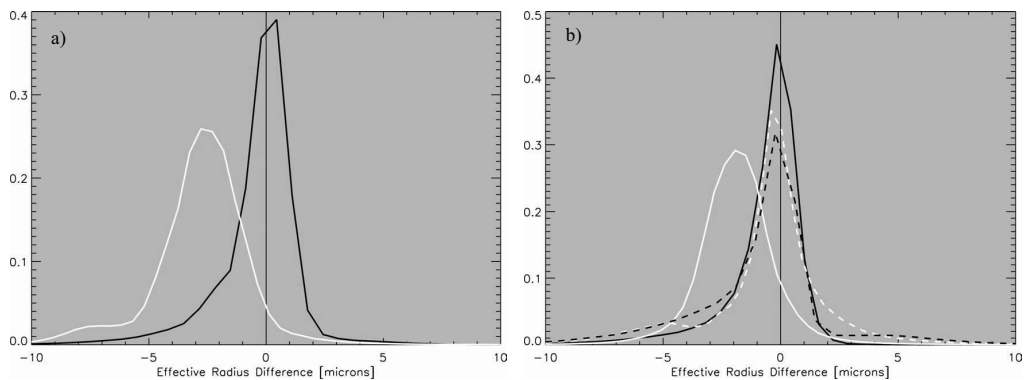


Figure 9. Probability density functions (pdfs) of  $r_{e1.63}-r_{e2.13}$  (white lines) and  $r_{e3.7}-r_{e2.13}$  (black lines) for: (a) 7 September, and (b) 10 September 2000. Solid lines represent the pdfs from aerosol-influenced pixels, and the dashed lines represent the pdfs from non-aerosol-influenced pixels.

TABLE 2. STATISTICS SHOWING THE MODAL EFFECTIVE RADIUS OF THE PDFS FOR AEROSOL- AND NON-AEROSOL-INFLUENCED PIXELS BOTH FOR  $r_{e1.63-r_{e2.13}}$  AND  $r_{e3.7-r_{e2.13}}$

Flight	Date	Mode of pdf ( $\mu\text{m}$ )				Approximate number of pixels $\times 1000$		
		aerosol		non-aerosol		aerosol	Indeterminate	non-aerosol
		$r_{e1.63-r_{e2.13}}$	$r_{e3.7-r_{e2.13}}$	$r_{e1.63-r_{e2.13}}$	$r_{e3.7-r_{e2.13}}$			
A785	5 Sept	-1.14	-0.15	-0.58	-0.31	425	450	460
A787	7 Sept	-2.78	+0.45	n/a	n/a	735	20	0
A788	10 Sept	-1.93	-0.17	-0.40	-0.22	705	115	490
A789	11 Sept	-1.02	-1.04	-0.04	-0.62	130	55	295
A791	14 Sept	-1.68	-1.40	+0.74	-0.86	185	85	330
A792	16 Sept	-1.32	+0.25	-0.10	-0.32	380	180	140

See text for details.

(iii) *TOMS AI*. A pixel is assigned as being ‘aerosol-influenced’ when the TOMS AI  $\geq 0.25$ , ‘non-aerosol-influenced’ when the TOMS AI  $\leq 0$ , and ‘indeterminate’ when  $0 < \text{TOMS AI} < 0.25$ .

We introduce the indeterminate classification to reduce misclassification of aerosol-influenced and non-aerosol-influenced pixels around the edges of the biomass burning aerosol plume, because the data from MODIS and TOMS are not exactly temporally collocated and a small amount of advection may have taken place. It would theoretically be possible to correlate  $r_{e1.63-r_{e2.13}}$  to TOMS AI, but inferences from such a correlation are made difficult by the variability in:  $\delta_{\text{cloud}}$ , cloud geometric height, aerosol above cloud, solar geometry, and satellite viewing geometry. Therefore we stick to our system of three classifications: aerosol-influenced, non-aerosol-influenced, and indeterminate pixels.

For 7 September, all of the area is affected by aerosol as shown by the statistics presented in Table 2; there are approximately 735 000 aerosol-influenced MODIS pixels and 20 000 indeterminate pixels, and zero non-aerosol-influenced pixels in the pdfs. Figure 9(a), therefore, shows only two pdfs associated with aerosol-influenced  $r_{e3.7-r_{e2.13}}$  and aerosol-influenced  $r_{e1.63-r_{e2.13}}$ . The modal value of  $r_{e3.7-r_{e2.13}}$  is slightly positive at  $+0.45 \mu\text{m}$  as expected from parcel theory. However, a value of  $r_{e1.63-r_{e2.13}}$  of  $-2.78 \mu\text{m}$  is greater in magnitude than any of the theoretical calculations of Platnick (2000) for clouds of similar optical depths, and appears significantly greater than the analysis of real MODIS data shown in Platnick *et al.* (2003), although no statistical analysis is shown in that work, which is again suggestive of the influence of overlying absorbing aerosol on the retrievals. Approximately 11% of aerosol-influenced pixels show a negative bias of  $|r_{e1.63-r_{e2.13}}|$  of more than  $5 \mu\text{m}$ , results that are difficult to explain unless overlying absorbing aerosol is affecting  $r_{e1.63}$ .

For 10 September, 705 000 pixels are assigned as being aerosol-influenced, 490 000 pixels are non-aerosol-influenced, and 115 000 indeterminate. Figure 9(b), therefore, shows four pdfs associated with  $r_{e3.7-r_{e2.13}}$  and  $r_{e1.63-r_{e2.13}}$  both for aerosol-influenced and for non-aerosol-influenced cases. Considering first  $r_{e3.7-r_{e2.13}}$ , the non-aerosol-influenced case shows a modal value of  $-0.22 \mu\text{m}$  and the aerosol-influenced case shows a modal value of  $-0.17 \mu\text{m}$ ; statistically there is no difference between these two values. The modal  $r_{e1.63-r_{e2.13}}$  for the non-aerosol-influenced pixels is relatively modest at  $-0.40 \mu\text{m}$ , which is consistent with the small negative bias associated with parcel theory, while the aerosol-influenced case shows a modal value of  $-1.93 \mu\text{m}$ . The mean bias for the aerosol-influenced pixels is  $-1.85 \mu\text{m}$  with a standard deviation of  $1.78 \mu\text{m}$  and therefore the mean bias is significant to  $1\sigma$ . Thus, by using TOMS AI to discriminate between aerosol-influenced and non-aerosol-influenced pixels, a bias in

$r_{e1.63}$  is revealed. The magnitude of this bias is somewhat less than the statistics suggest for aerosol-influenced pixels for 7 September; this might be expected because the TOMS AI and  $\delta_{\text{aerosol}}$  for 10 September is somewhat smaller than for 7 September.

The results of the statistical analysis for the rest of the cases examined here (5, 11, 14 and 16 September) are summarized in Table 2. The results for  $r_{e3.7}-r_{e2.13}$  show a slightly negative bias for the non-aerosol-influenced pixels, but when aerosol-influenced pixels are considered  $r_{e3.7}-r_{e2.13}$  can be either more positive or more negative. The results for  $r_{e1.63}-r_{e2.13}$  are quite different; in all cases the non-aerosol-influenced pixels show more positive values than the aerosol-influenced pixels. This provides further evidence that overlying aerosol is influencing the retrieval of  $r_{e1.63}$ .

## 7. DISCUSSION AND CONCLUSIONS

Using realistic aerosol properties and reasonable relative positions of aerosol and cloud, we perform model radiative transfer calculations that show that satellite retrievals of  $\delta_{\text{cloud}}$  are likely to be underestimated in regions that are affected by overlying partially absorbing aerosol. This result is despite the fact that an additional  $\delta_{\text{aerosol}}$  of 0.5 at  $0.55 \mu\text{m}$  is included in the calculations, leading to a larger  $\delta_{\text{total}}$ .

We also show that the combination of 0.86/1.63  $\mu\text{m}$  radiances/reflectances used in MODIS retrievals is theoretically susceptible to producing an underestimate in  $r_{e1.63}$  in regions of overlying partially absorbing aerosol. These results are backed up by a practical analysis of the MODIS data for six cases (two cases presented in detail) where overlying biomass aerosol exists above stratocumulus clouds. Platnick *et al.* (2003), investigating an example of stratocumulus off the western coast of Chile and Peru, show that  $|r_{e1.63}-r_{e2.13}|$  is often within  $1 \mu\text{m}$  although some significant differences exist of around  $\sim -2.5 \mu\text{m}$ . It is suggested that these differences are associated with parcel theory (Platnick *et al.* 2003), whereby the  $1.63 \mu\text{m}$  reflectance is less affected by water droplet absorption than the  $2.13 \mu\text{m}$  reflectance, and therefore probes deeper in the cloud where cloud droplets tend to be smaller. The theoretical calculations using cloud droplet distributions with an  $r_e$  that does not vary in the vertical, suggest systematic biases in  $|r_{e2.13}-r_{e1.63}|$  of as much as  $5 \mu\text{m}$ , which generally exceeds the differences that might be expected from parcel theory. By using the TOMS AI to delineate regions that are/are not affected by aerosols, we show: firstly a modal bias in  $r_{e1.63}-r_{e2.13}$  of as much as  $-2.78 \mu\text{m}$ ; secondly statistical analyses suggesting that  $|r_{e2.13}-r_{e1.63}|$  is greater than  $-5 \mu\text{m}$  for as much as 11% of aerosol-influenced pixels; and thirdly spatial structures in the biases of  $r_{e2.13}-r_{e1.63}$  that appear correlated to the presence of overlying aerosol. These results support the theoretical calculations, suggesting that not only the vertical distribution of cloud droplet size but also overlying partially absorbing aerosol are responsible for the smaller value of  $r_{e1.63}$  compared to  $r_{e2.13}$  and  $r_{e3.7}$ . It might be argued that the presence of the overlying absorbing aerosol might change the dynamical evolution of stratocumulus, thereby affecting the cloud geometric height and  $r_e$  (Johnson *et al.* 2004). However, both this semi-direct and the indirect effect should not lead to significant wavelength-dependent differences in  $r_e$ , and are thus unlikely to explain the result that  $r_{e1.63}$  has a low bias in regions affected by aerosol.

Our results for biomass burning aerosol are somewhat better constrained than the results for mineral dust aerosol, because we have reasonable statistics for determining the aerosol and underlying stratocumulus cloud properties, while in the regions where Saharan dust outbreaks are frequent the cloud is much more variable in nature. Because of this variability, we do not present an analysis of MODIS data for the SHADE period. However, the assumptions made in determining the radiances for Saharan dust aerosol

appear reasonable. While our results are applicable to the Namibian/Angolan stratocumulus regions and regions affected by Saharan dust outbreaks, absorbing aerosol above low cloud is experienced in a number of other regions, such as the pollution advected from eastern Asia studied during the Aerosol Characterisation Experiment (ACE-Asia, Hsu *et al.* 2003). The CALIPSO (Cloud–Aerosol Lidar and Infrared Pathfinder Satellite Observations) instrument may have an important role in clarifying the effects of different types of overlying aerosol upon cloud physical parameter retrievals (Winker *et al.* 2003).

One of the largest sources of uncertainty in determining the direct radiative impact of aerosols stems from the lack of knowledge of the aerosol  $\omega_{0\lambda}$ , which determines whether an aerosol heats or cools the atmosphere (e.g. Haywood and Boucher 2000). For example, considerable uncertainty has recently been highlighted in the absorption properties of mineral dust, with recent *in situ* and remote sensing methods suggesting a much lower degree of absorption than previously thought (e.g. Kaufman *et al.* 2001; Haywood *et al.* 2003b). It might be possible to determine  $\omega_{0\lambda}$  by performing retrievals where the 1.63  $\mu\text{m}$  reflectance is combined with reflectances from other MODIS bands in the spectral range 0.4–0.75  $\mu\text{m}$  (MODIS has 11 bands in this range), and consistency of the modelled optical properties including  $\omega_{0\lambda}$  could be assessed. A low bias in the retrieved  $r_e$  will only be evident if the aerosol is significantly absorbing. Variability in cloud and aerosol optical properties and vertical profiles may make this sort of analysis difficult in practice.

An important conclusion from this study is that those wishing to investigate the indirect effect of aerosols upon cloud in these regions via remote sensing techniques should be aware of this ‘apparent indirect effect’, whereby anomalously low values of  $r_{e1.63}$  are retrieved due to the presence of *overlying* absorbing aerosols, rather than the influence of aerosols upon the cloud microphysics.

#### ACKNOWLEDGEMENTS

We would like to thank the Meteorological Research Flight aircrew and support staff for their efforts during SAFARI 2000. Peter Francis is thanked for his input to this work, and for reading an earlier version of the manuscript. John Edwards is thanked for development and maintenance of the radiative transfer code. Steve Platnick is thanked for his extremely valuable comments regarding the MODIS retrieval algorithms and MODIS products. Steven Abel would like to thank NERC and the Met Office for providing the CASE studentship under which this research was undertaken.

#### REFERENCES

- |   |      |  |
|---|------|--|
| Edwards, J. M. and Slingo, A.   | 1996 | Studies with a flexible new radiation code. I: Choosing a configuration for a large-scale model. <i>Q. J. R. Meteorol. Soc.</i> , <b>122</b> , 689–720   |
| Fouquart, Y., Bonnel, B.,<br>Brogniez, G., Buriez, J. C.,<br>Smith, L. and Morcrette, J. J. | 1987 | Observations of Saharan aerosols: Results of ECLATS field experiment. Part II: Broadband radiative characteristics of aerosols and vertical flux divergence. <i>J. Clim. Appl. Meteorol.</i> , <b>26</b> , 38–52 |
| Garrett, T. J. and Hobbs, P. V.   | 1995 | Long-range transport of continental aerosols over the Atlantic Ocean and their effects on cloud structure. <i>J. Atmos. Sci.</i> , <b>52</b> , 2977–2984   |
| Glew, M. D., Hignett, P. and<br>Taylor J. P.  | 2004 | Aircraft measurements of sea surface albedo. <i>J. Atmos. Sci.</i> , in press  |
| Han, Q., Rossow, W. B. and<br>Lacis, A. A.  | 1994 | Near-global survey of effective droplet radii in liquid water clouds using ISCCP data. <i>J. Climate</i> , <b>7</b> , 465–497  |
| Han, Q., Rossow, W. B., Chou, J.<br>and Welch, R. M.  | 1998 | Global variation of column droplet concentration in low-level clouds. <i>Geophys. Res. Lett.</i> , <b>25</b> , 1419–1422   |

- Haywood, J. M. and Boucher, O. 2000 Estimates of the direct and indirect radiative forcing due to tropospheric aerosols: A review. *Revs Geophys.*, **38**, 513–543
- Haywood, J. M. and Osborne, S. R. 2000 ‘Corrections to be applied to the PSAP and nephelometer for accurate determination of the absorption coefficient, scattering coefficient and single scattering albedo’. MRF Technical Note No 31. Available from: Met Office, Y46 Bldg, Cody Technology Park, Farnborough, Hants, GU14 0LX, UK
- Haywood, J. M. and Shine, K. P. 1995 The effect of anthropogenic sulfate and soot aerosol on the clear sky planetary radiation budget. *Geophys. Res. Lett.*, **22**, 603–606
- Haywood, J. M., Osborne, S. R., Francis, P. N., Keil, A., Formenti, P., Andreae, M. O. and Kaye, P. H. 2003a The mean physical and optical properties of regional haze dominated by biomass burning aerosol measured from the C-130 aircraft during SAFARI 2000. *J. Geophys. Res.*, **108**(D13), 8473, doi:10.1029/2002JD002226
- Haywood, J. M., Osborne, S. R., Francis, P., Glew, M., Highwood, E., Formenti, P. and Andreae, M. 2003b Radiative properties and direct radiative effect of Saharan dust measured by the C-130 aircraft during SHADE: 1. Solar spectrum. *J. Geophys. Res.*, **108**(D13), 8577, doi:10.1029/2002JD002687
- Haywood, J. M., Francis, P. N., Glew, M. D., Dubovik, O. and Holben, B. N. 2003c Comparison of aerosol size distributions, radiative properties, and optical depths determined by aircraft observations and sun photometers during SAFARI-2000. *J. Geophys. Res.*, **108**(D13), 8471, doi:10.1029/2002JD002250
- Highwood, E. J., Haywood, J. M., Silverstone, M. D., Newman, S. M. and Taylor, J. P. 2003 Radiative properties and direct effect of Saharan dust measured by the C-130 aircraft during SHADE. 2: Terrestrial spectrum. *J. Geophys. Res.*, **108**(D18), 8578, doi:10.1029/2002JD002552
- Hobbs, P. V. 2002 Clean air slots amid atmospheric pollution. *Nature*, **415**, 861
- Hsu, N. C., Herman, J. R., Torres, O., Holben, B. N., Tanré, D., Eck, T. F., Smirnov, A., Chatenet, B. and Lavenu, F. 1999 Comparison of the TOMS aerosol index with sun-photometer aerosol optical thickness: Results and applications. *J. Geophys. Res.*, **104**, 6269–6279
- Hsu, N. C., Herman, J. R. and Chen, S.-C. 2003 Radiative impacts from biomass burning in the presence of clouds during boreal spring in southeast Asia. *Geophys. Res. Lett.*, **30**(5), 1224, doi:10.1029/2002GL016485
- Johnson, B. T., Shine, K. P. and Forster, P. M. 2004 The semi-direct aerosol effect: Impact of absorbing aerosols on marine stratocumulus. *Q. J. R. Meteorol. Soc.*, in press
- Kaufman, Y., Tanré, D., Dubovik, O., Karnieli, A. and Remer, L. A. 2001 Absorption of sunlight by dust as inferred from satellite and ground-based remote sensing. *Geophys. Res. Lett.*, **28**, 1479–1483
- Kaufman, Y., Haywood, J. M., Hobbs, P. V., Hart, W., Kleidman, R. and Schmid, B. 2003 Remote sensing of vertical distribution of smoke aerosol off the coast of Africa during SAFARI 2000. *Geophys. Res. Lett.*, **30**, 1831, doi:10.1029/2003GL017068
- Keil, A. and Haywood, J. M. 2003 Solar radiative forcing by biomass aerosol particles over marine clouds during SAFARI-2000. *J. Geophys. Res.*, **108**(D13), 8467, doi:10.1029/2002JD002315
- King, M. D., Menzel, W. P., Kaufman, Y. J., Tanré, D., Gao, B.-C., Platnick, S., Ackerman, S. A., Remer, L. A., Pincus, R. and Hubanks, P. A. 2003 Cloud and aerosol properties, precipitable water and profiles of temperature and water vapor from MODIS. *IEEE Trans. Geosci. Remote Sensing*, **41**, 442–458, doi:10.1109/TGRS.2002.808226
- Liao, H. and Seinfeld, J. H. 1998 Radiative forcing by mineral dust aerosol: Sensitivity to key variables. *J. Geophys. Res.*, **103**, 31637–31646
- McClatchey, R. A., Fenn, R. W., Selby, J. E. A., Volz, P. E. and Garing, J. S. 1972 ‘Optical properties of the atmosphere (third edition)’. Research paper 411, Air Force Cambridge, MA, USA
- Myhre, G., Berntsen, T. K., Haywood, J. M., Sundet, J. K., Holben, B. N., Johnsrud, M. and Stordal, F. 2003 Modelling the radiative impact of aerosols from biomass burning during SAFARI-2000. *J. Geophys. Res.*, **108**(D13), 8501, doi:10.1029/2002JD002313
- Platnick, S. 2000 Vertical photon transport in cloud remote sensing problems. *J. Geophys. Res.*, **105**(D18), 22919–22935
- Platnick, S., King, M. D., Ackerman, S. A., Menzel, W. P., Baum, B. A., Riédi, J. C. and Frey, R. A. 2003 The MODIS cloud products: algorithms and examples from Terra. *IEEE Trans. Geosci. Remote Sensing*, **41**, 459–473, doi:10.1109/TGRS.2002.808301

- Sokolik, I. N., Toon, O. B. and Bergstrom, R. W. 1998 Modelling the radiative characteristics of airborne mineral aerosols at infrared wavelengths. *J. Geophys. Res.*, **103**, 8813–8826
- Tanré, D., Haywood, J. M., Pelon, J., Léon, J. F., Chatenet, B., Formenti, P., Francis, P., Goloub, P., Highwood, E. J. and Myhre, G. 2003 Measurement and modeling of the Saharan dust radiative impact: Overview of the SaHaran Dust Experiment (SHADE). *J. Geophys. Res.*, **108**(D13), 8574, doi:10.1029/2002JD003273
- Winker, D. M., Pelon, J. and McCormick, M. P. 2003 The CALIPSO mission: Spaceborne lidar for observation of aerosols and clouds. *Proc. SPIE*, **4893**, 1–11
- WMO 1986 'A preliminary cloudless standard atmosphere for radiation computation'. World Climate Program of the World Meteorological Organization, Geneva, Switzerland